Nanoscale

PAPER

View Article Online
View Journal | View Issue



Cite this: *Nanoscale*, 2018, **10**, 16759

# Band gap reduction in van der Waals layered 2D materials *via* a de-charge transfer mechanism†

Chunxiao Zhang,[a,b] Huaqing Huang,[b] Xiaojuan Ni,[b] Yinong Zhou,[b] Lei Kang,[b] Wei Jiang,[b] Haiyuan Chen,[b] Jianxin Zhong*[a] and Feng Liu*[b,c]

Received 8th June 2018,
Accepted 7th August 2018

DOI: 10.1039/c8nr04660c

rsc.li/nanoscale

A thickness dependent band gap is commonly found in layered two-dimensional (2D) materials. Here, using a $C_3N$ bilayer as a prototypical model, we systematically investigated the evolution of a band gap from a single layer to a bilayer using first principles calculations and tight binding modeling. We show that in addition to the widely known effect of interlayer hopping, de-charge transfer also plays an important role in tuning the band gap. The de-charge transfer is defined with reference to the charge states of atoms in the single layer without stacking, which shifts the energy level and modifies the band gap. Together with band edge splitting induced by the interlayer hopping, the energy level shifting caused by the de-charge transfer determines the size of the band gap in bilayer $C_3N$. Our finding, applicable to other 2D semiconductors, provides an alternative approach for realizing band gap engineering in 2D materials.



## 1. Introduction

Band gap is a fundamental parameter that governs the transport and light–matter interaction properties in condensed matter systems. For two-dimensional (2D) materials, constructing van der Waals layered structures is a practical route to tailor the electronic properties.[1–5] Along with other advances, such as the preserved ideal properties of isolated components[6–9] and gate-tunable band structures,[10–15] the band gap is found to generally decrease and even undergo a semiconductor–metal transition with the increasing thickness in van der Waals layered structures. This phenomenon is often attributed to the prevailing mechanism of energy splitting of band edges caused by the interlayer hopping as reported in previous studies.[16–19] However, this mechanism can be insufficient to explain the observed considerable band gap decrease. Thus, there should be other hidden mechanisms to also account for the overall band gap reduction.

Besides hopping, charge transfer is an important factor to modify the band gap as it causes the shifting of energy levels. Considering that in a hexagonal lattice with the same electronic energy at all the sites, as in graphene,[20] a uniform π-conjugation is formed, resulting in a semimetal with zero band gap. When introducing an electrostatic potential asymmetry (on-site energy difference) in the lattice, such as the case in BN and $C_3N$,[21,22] the charge transfer will open a (charge) gap in proportion to this on-site energy (chemical potential) difference. Conversely, a de-charge transfer mechanism can be triggered by reducing/removing the site chemical potential difference, so that the gap will be decreased/closed. Here, we demonstrate that the de-charge transfer may ubiquitously function to affect the band gap of van der Waals layered 2D compound materials.

We take $C_3N$[22,23] as an example to investigate the effect of de-charge transfer on its band gap using the first-principles calculations with the hybrid functional (HSE06) and a tight-binding (TB) model with the nearest-neighbor (NN) hopping. $C_3N$, as shown in Fig. 1(a), is a new promising 2D material with a graphene-like honeycomb lattice. Single-layer $C_3N$ has a medium band gap of about 1 eV at the HSE level. Its band gap decreases sharply in the bilayer and undergoes a semiconductor–metal transition when the number of layers is beyond three.[19] In this paper, we first show the dependence of the band gap on charge transfer in the single layer, then give a general description of de-charge transfer and band gap reduction in the bilayer based on the TB model. Secondly, we demonstrate the effects of de-charge transfer on the band gap in the $C_3N$ bilayer based on the density functional theory (DFT) calculation and TB model.

[a]*Hunan Provincial Key Laboratory of Micro-Nano Energy Materials and Devices, Xiangtan University, Hunan 411105, People's Republic of China. E-mail: jxzhong@xtu.edu.cn; Fax: +86 732 58292468; Tel: +86 732 52665818*
[b]*Department of Materials Science and Engineering, University of Utah, Salt Lake City, UT 84112, USA. E-mail: fliu@eng.utah.edu*
[c]*Collaborative Innovation Center of Quantum Matter, Beijing, 100084, People's Republic of China*

†Electronic supplementary information (ESI) available. See DOI: 10.1039/c8nr04660c

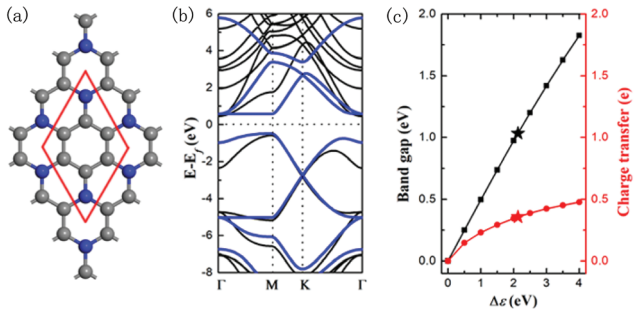


Fig. 1 (a) Top view of the crystal structure of monolayer $C_3N$. Red dashed lines indicate the primitive cell. (b) Tight-binding fitting (blue-solid lines) of the HSE bands (black-solid lines) for monolayer $C_3N$. Tight-binding fitting was made for the $p_z$ bands with the NN hopping. (c) The evolution of the band gap and charge transfer with $\Delta\varepsilon$ based on the tight-binding simulation. Black and red curves represent the band gap and charge transfer, respectively.

## 2. Methods

First-principles calculations are performed based on the Kohn–Sham density functional theory (DFT)[24] using the Vienna *ab initio* simulation package (VASP).[25] The generalized gradient approximation within the Perdew–Burke–Ernzerhof (PBE) functional form[26] is used for the exchange–correlation energy. To describe correctly van der Waals interactions within $C_3N$ layers, a correction term (DFT-D2 method of Grimme[27]) is further added when calculating the conventional Kohn–Sham potential energy and interatomic forces. The DFT-D2 correction has been documented to well describe the graphite system[28] which is a structural analogue of $C_3N$. A plane-wave cutoff of 600 eV is used to expand the valence electron wave functions. All atomic positions and lattice vectors are fully optimized using a conjugate gradient algorithm to obtain the ground-state configuration. Atomic relaxation is performed until the change of total energy is smaller than 0.001 meV and the Hellmann–Feynman force on each atom is less than 0.005 eV Å$^{-1}$. A vacuum space of 20 Å is maintained in the *z*-axis to avoid mirror interactions. The Brillouin zone is represented by a Monkhorst–Pack[29] special *k*-point mesh of 7 × 7 × 1 for geometry optimization and SCF computations. As the PBE functional is well known to underestimate the band gap, the more accurate HSE06 functional[30,31] is used to correct this underestimation.

## 3. Results and discussion

### 3.1. Tight-binding model and charge transfer in the $C_3N$ single layer

We present the tight-binding model and parameters for the $C_3N$ single layer by fitting with the DFT bands in this section. Fig. 1(a) shows the optimized structure of the $C_3N$ single layer. It can be considered that in $C_3N$ two carbon atoms are substituted by nitrogen atoms within the *P6/mmm* symmetry in a 2 × 2 graphene supercell, and the lattice constant is shrunk from 4.92 Å to 4.86 Å. All carbon and nitrogen atoms are $sp^2$ hybridized, forming conjugated π-bonds. The same length is found for C–C (1.403 Å) and C–N (1.403 Å) bonds. From band structures shown in Fig. 1(b), we find that $C_3N$ is a semiconductor with an indirect band gap of 1.04 eV. The valence band maximum (VBM) locates at the *M* point and the conductance band minimum (CBM) locates at the *Γ* point, in agreement with previous results.[19]

Since the bands near the Fermi level are dominated by the π conjugation, we employ a TB model involving the $p_z$–$p_z$ interaction with the NN hopping to describe the $C_3N$ single layer. The following eight-band model is used:

$$H = \sum_i \varepsilon_C n_i + \sum_j \varepsilon_N n_j + \sum_{i\neq j} t^{\parallel} c_i^{\dagger} c_j \quad (1)$$

where the summation runs over the lattice sites (six carbon sites and two nitrogen sites per unit cell). $\varepsilon_C$ and $\varepsilon_N$ are the on-site energy at carbon and nitrogen sites, respectively. $t^{\parallel}$ is the in-plane hopping parameter, and $c_i^{\dagger}(c_j)$ is the creation (annihilation) operator of electrons at site $i(j)$. Because we focus on the charge transfer caused by the on-site energy difference, the parameter $t^{\parallel}$ is set to be 3.1 eV as in graphene.[32,33] We obtain the optimized on-site energy, $\varepsilon_C = -2.6$ and $\varepsilon_N = -4.73$, by fitting to the HSE bands as shown in Fig. 1(b). We note that the TB bands shown in Fig. 1b reproduce the most salient features of DFT bands, especially in terms of band gap size at high-symmetry *k*-points. However, quantitatively there are notable differences between them. It is possible to significantly improve the TB bands to better agree with the DFT bands by adding up to 3NN hopping (see the ESI†), but it will not affect the de-charge mechanism we discuss here. In comparison with graphene, one more band is occupied and the Dirac cone shifts below the Fermi level, since two more π electrons are present in the $C_3N$ primitive cell than in the 2 × 2 graphene supercell, so that the Fermi level is located between the fifth and sixth band in our TB band structure.

To describe the charge transfer ($\Delta e$) in the $C_3N$ single layer, we calculate the electron density at each site based on the TB model. The TB Hamiltonian can operate in the space of coefficients of the TB function $c(\vec{k}) = (c_{N_1}, c_{C_1}, c_{C_2}, c_{C_3}, c_{C_4}, c_{C_5}, c_{C_6}, c_{N_2})$ where $c_{C_i} = c_{C_i}(\vec{k})$ and $c_{N_i} = c_{N_i}(\vec{k})$ are the coefficients for C and N atoms, respectively. The total eigenfunction of the system is then given by:

$$\Psi = \sum_{i=1}^{6} c_{C_i} \psi_{\vec{k}}^{C_i}(\vec{r}) + \sum_{j=1}^{2} c_{N_j} \psi_{\vec{k}}^{N_j}(\vec{r}) \quad (2)$$

The eight coefficients in eqn (2), for the fixed value of $t^{\parallel}$, can be obtained by diagonalizing a Hamiltonian matrix. Based on the coefficients, the electronic density at each carbon and nitrogen site is given by:

$$n_{C_i} = \sum_{n=1}^{N_b} \iint |c_{n,C_i}|^2 \mathrm{d}k_x \mathrm{d}k_y \quad (3)$$

$$n_{N_j} = \sum_{n=1}^{N_b} \iint |c_{n,N_j}|^2 dk_x dk_y \quad (4)$$

where $N_b$ is the number of occupied bands and $N_b = 5$ in the $C_3N$ single layer. The charge transfer is determined to be the variation of the electron density at the nitrogen site as follows:

$$\Delta e = n_{N_j} - n_0 \quad (5)$$

where $n_0$ is the electron density at each site in a system with the electrostatic potential symmetry, *i.e.*, the on-site energies are equal at all the sites and the π electrons uniformly distribute in the single layer with $n_0 = 1.25e$ at each site.

In Fig. 1(c) we show the dependence of the $\Delta e$ and band gap on the on-site energy difference ($\Delta\varepsilon = \varepsilon_C - \varepsilon_N$) with $\varepsilon_C$ being fixed at −2.6 eV. The origin point corresponds to the system with the electrostatic potential symmetry. From Fig. 1(c), one can see that both the $\Delta e$ and band gap increase with the $\Delta\varepsilon$. The on-site energy difference induces the charge transfer from carbon to nitrogen sites, which shifts the energy levels near the Fermi level and then opens a band gap. The stars indicate the charge transfer and band gap in the $C_3N$ single layer where $0.34e$ of electrons transfer into each nitrogen site. From the Bader charge analysis[34] based on the DFT calculation, we found that 0.4 electrons transfer into the $p_z$ state of each nitrogen atom in reasonably good agreement with the TB estimation.

### 3.2. General description for band gap reduction and de-charge transfer in the bilayer

A simplified TB model is used to give a general description for the band gap and de-charge transfer in the van der Waals bilayer. Based on the first-principles energy calculations, the AD stacking shown in Fig. 2(a) is the most stable form of $C_3N$ bilayer (the stability of the $C_3N$ bilayer is discussed in detail in the ESI†). In AD stacking, the top layer is directly stacked on the bottom layer, but the top layer of atoms is shifted by a half primitive cell along the armchair direction. The inter-layer spacing is 3.175 Å, corresponding to the van der Waals interaction. In the TB model, the bilayer is modeled as two coupled single-layer $C_3N$ hexagonal lattices with an additional inter-layer hopping, arranged according to AD stacking. For simplicity, the NN inter-layer hopping is considered with equal magnitude, which is qualitatively good enough for now. The TB Hamiltonian reads:

$$H = \sum_i \varepsilon_C n_i + \sum_j \varepsilon_N n_j + \sum_{i\neq j} t^{\parallel} c_i^{\dagger} c_j + \sum_{i\neq j} \gamma c_i^{\dagger} c_j \quad (6)$$

where the first three items have the same meaning as in eqn (1), while the fourth item describes the inter-layer interaction. Fig. 2(b) shows the evolution of the band gap as functions of both inter-layer hopping ($\gamma$) and in-plane on-site energy difference ($\Delta\varepsilon$). We find that either increasing $\gamma$ or decreasing $\Delta\varepsilon$ can reduce the band gap. For example, keeping $\Delta\varepsilon$ to be 2.13 eV as the value in the $C_3N$ single layer the band gap is closed by increasing the inter-layer hopping to $\gamma = 0.54$ eV, while upon neglecting the inter-layer hopping the band gap would be closed without the on-site energy difference.

The electron densities of individual atoms are obtained by using eqn (3) and (4) with $N_b = 10$. The amount of de-charge transfer is also determined by calculating the change of electrons at each nitrogen site:

$$\Delta e = n_N - n_{N_j} \quad (7)$$

where $n_N$ is the electron density of the nitrogen site in the $C_3N$ single layer which is $1.59e$ as obtained by using eqn (4) with $N_b = 5$. $n_{N_j}$ is the electron density of each nitrogen site in the bilayer. Because both $\gamma$ and $\Delta\varepsilon$ can modify the band gap, we study the dependence of de-charge transfer on $\gamma$ and $\Delta\varepsilon$, respectively. As shown in Fig. 3(a), the de-charge transfer is almost independent of $\gamma$. For instance, when increasing $\gamma$ from 0 eV to 0.4 eV and keeping $\Delta\varepsilon$ at 1.63 eV, the de-charge transfer only changes from $0.050e$ to $0.057e$, but the band gap significantly decreases from 0.807 eV to 0.022 eV. On the other hand, the de-charge transfer almost linearly increases with $\Delta\varepsilon$. For instance, keeping $\gamma$ at 0.3 eV, $0.072e$ of de-charge transfer occurs from N to C and the band gap is reduced from 0.457 eV

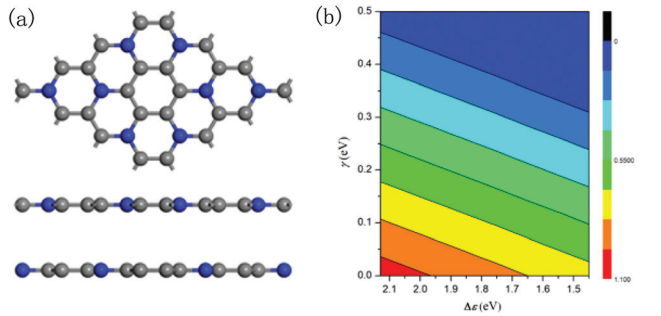


Fig. 2 (a) Top and side view of the crystal structure of the AD-stacked $C_3N$ bilayer. Blue and gray balls represent nitrogen and carbon atoms, respectively. (b) Evolution of the band gap with both $\gamma$ and $\Delta\varepsilon$.

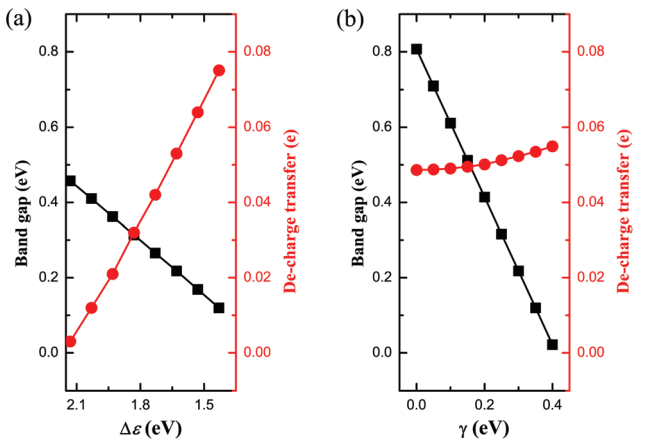


Fig. 3 (a) The dependence of both de-charge transfer and band gap on $\gamma$ when $\Delta\varepsilon^{\parallel} = 1.63$ eV. (b) The dependence of both de-charge transfer and band gap on $\Delta\varepsilon^{\parallel}$ when $\gamma = 0.3$ eV. Black and red curves represent the band gap and de-charge transfer, respectively.

to 0.12 eV, when $\Delta\varepsilon$ is decreased from 2.13 eV to 1.43 eV, as shown in Fig. 3(b). In general, we find that inter-layer hopping reduces the band gap by inducing energy splitting of band edges while de-charge transfer reduces the band gap by shifting the energy level near the Fermi level.

### 3.3. The mechanism of thickness dependent band gap tuning in the $C_3N$ bilayer

In this section, we illustrate the effects of de-charge transfer on the thickness dependent band gap of the $C_3N$ bilayer based on both DFT calculations and TB modeling in detail. To describe the de-charge transfer in the $C_3N$ bilayer based on the DFT calculations, we analyze the redistribution of charge density ($\Delta\rho_e$) which is determined as follows:

$$\Delta\rho_e = \rho_{bilayer} - 2\rho_{monolayer} \quad (8)$$

where $\rho_{bilayer}$ and $\rho_{monolayer}$ are the charge density of the $C_3N$ bilayer and isolated $C_3N$ single layer, respectively. The distribution of $\Delta\rho_e$ is shown in Fig. 4(a). One can see that the distribution of $\Delta\rho_e$ is symmetric between the two layers. A depletion of charge density is found in the $p_z$ state of nitrogen and its neighboring carbon atoms in the armchair direction, while an accumulation of the charge density is found in the $p_z$ state of other carbon atoms. The charge mainly transfers back from nitrogen atoms with high electron negativity to carbon atoms with low electron negativity in the zigzag direction, which manifests the de-charge transfer. The evolution of the de-charge transfer with inter-layer spacing is shown in Fig. 4(b). We find that when the interlayer spacing is enlarged by 1.2 Å relative to the $C_3N$ bilayer, the interlayer interaction becomes so weak that each layer could be considered as an isolated single layer. In that case, the band gap is almost equal to that of the $C_3N$ single layer and the de-charge transfer is close to zero. Reducing the interlayer spacing gives rise to the interlayer interaction which results in both band gap reduction and de-charge transfer. For instance, the band gap is reduced to 0.89 eV while 0.031$e$ of electrons transfer out of each N-$p_z$ (calculated based on the Bader charge analysis) when the interlayer spacing decreases to 3.175 Å.

Finally, we further clarify the mechanism of the thickness dependent band gap based on the TB model. From the distribution of the charge density and the electron density at individual sites, we introduce different on-site energies at two nonequivalent carbon sites ($C_1$ and $C_2$) in each layer, as well as two different interlayer hoppings (C–N interlayer hopping $\gamma_1$ and C–C interlayer hopping $\gamma_2$) as shown in Fig. 5(a). The band structure of $C_3N$ is shown in Fig. 5(b). From the HSE band structures, we find that the degeneracy between $K_1$ and $K_2$ ($M_1$ and $M_2$) is removed because of the breaking of the inversion symmetry in comparison with the $C_3N$ single layer. The $C_3N$ bilayer is also an indirect semiconductor with the VBM and CBM located at $M_2$ and $\Gamma$, respectively, but the band gap decreases from 1.04 eV to 0.089 eV. Fitting the TB bands to the HSE results, we find that the energy splitting near the Fermi level mainly originates from the interlayer hopping. By fitting the energy splitting to the DFT results at the band edges, $\gamma_1$ and $\gamma_2$ are obtained as 0.42 eV and 0.3 eV, respectively. Upon keeping all the on-site energies as the values in the $C_3N$ single layer, when $\gamma_1$ and $\gamma_2$ are set to be 0.42 eV and 0.3 eV, the band gap decreases from 1.04 eV to 0.336 eV but the de-charge transfer is just 0.002$e$ compared with the $C_3N$ single layer. It indicates that the interlayer hopping is indeed an important factor to tune the band gap but has little effect on the de-charge

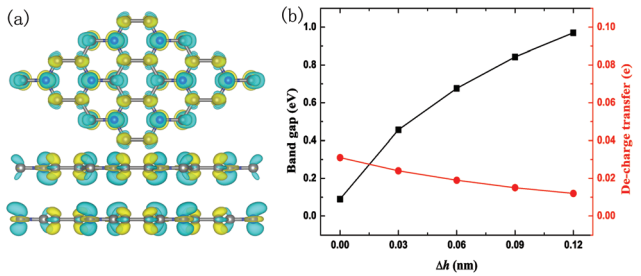


Fig. 4 (a) The redistribution of the charge density in bilayer $C_3N$. Blue and yellow isosurfaces correspond to the positive and negative values of $2 \times 10^{-3}$ e Å$^{-1}$. (b) The dependence of the band gap and de-charge transfer on the interlayer spacing. The de-charge transfer is calculated based on the Bader charge analysis and $\Delta h$ is the variation of the interlayer spacing relative to the $C_3N$ bilayer.

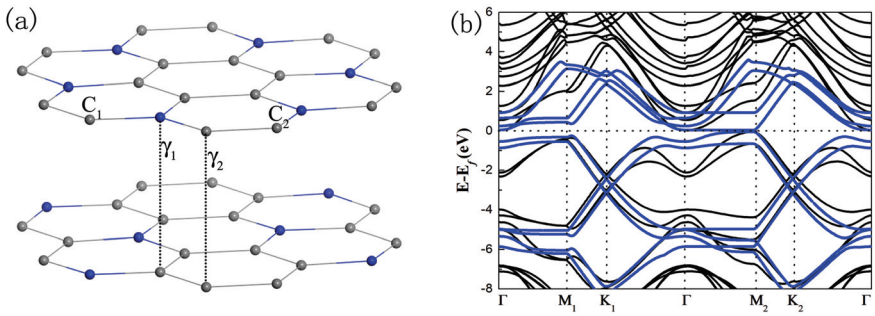


Fig. 5 (a) Schematic of the bilayer lattice containing two nonequivalent carbon sites and two different interlayer hoppings in the unit cell. (b) Tight-binding fitting (blue-solid lines) of the HSE bands (black-solid lines) for bilayer $C_3N$. Tight-binding fitting was made for the $p_z$ bands within NN hopping. The differences of interlayer hopping and the on-site energy of nonequivalent carbon sites are considered.

 

transfer. The band gap of 0.336 eV is still much larger than the DFT band gap (0.089 eV at the HSE level) of the $C_3N$ bilayer. In order to fit the band gap with the DFT result, the on-site energies are then modified to −4.33 eV, −2.50 eV and −2.60 eV at the N, $C_1$ and $C_2$ sites, respectively. Based on these TB parameters, the de-charge transfer is calculated to be 0.036*e* using eqn (7), which agrees with the result of the Bader charge analysis. So the de-charge transfer induces about 0.247 eV additional band gap reduction. Consequently, in the $C_3N$ bilayer the inter-layer interaction not only induces the inter-layer hopping but also changes the in-plane on-site energy. The variation of the in-plane on-site energy difference causes the de-charge transfer which shifts the energy level near the Fermi level. Together with energy splitting induced by inter-layer hopping, de-charge transfer is another important parameter for tuning the band gap.

## 4. Conclusion

We propose that de-charge transfer provides an important mechanism for band engineering of van der Waals layered 2D materials, in addition to interlayer hopping. We reveal this mechanism by a systematic study of the band gap of a $C_3N$ bilayer as a model system using first principles calculations and tight-binding modeling. We believe this mechanism is generally applicable to all the 2D semiconductor homo- and hetero-junctions. Our findings will be not only fundamentally useful to better understand the band gap evolution of 2D materials as a function of thickness, but also practically significant for band gap engineering of 2D materials.

## Conflicts of interest

There are no conflicts to declare.

## Acknowledgements

This work is supported by the National Natural Science Foundation of China (Grant No. 11474244), the Program for Chang Jiang Scholars and Innovative Research Team in University (IRT13093), and the Natural Science Foundation of Hunan Province of China (Grant No. 2016JJ3118). H. H., X. N., Y. Z., and F. L. are supported by the U.S. DOE-BES (Grant No. DE-FG02-04ER46148). We also acknowledge financial support from the China Scholarship Council. The calculations were partly done at the CHPC at the University of Utah, United States of America.

## References

1 H. Wang, L. Yu, Y.-H. Lee, Y. Shi, A. Hsu, M. L. Chin, L.-J. Li, M. Dubey, J. Kong and T. Palacios, *Nano Lett.*, 2012, **12**, 4674–4680.
2 C.-J. Shih, Q. H. Wang, Y. Son, Z. Jin, D. Blankschtein and M. S. Strano, *ACS Nano*, 2014, **8**, 5790–5798.
3 Y. Deng, Z. Luo, N. J. Conrad, H. Liu, Y. Gong, S. Najmaei, P. M. Ajayan, J. Lou, X. Xu and P. D. Ye, *ACS Nano*, 2014, **8**, 8292–8299.
4 M. Bernardi, M. Palummo and J. C. Grossman, *Nano Lett.*, 2013, **13**, 3664–3670.
5 M. M. Furchi, A. Pospischil, F. Libisch, J. Burgdorfer and T. Mueller, *Nano Lett.*, 2014, **14**, 4785–4791.
6 G. Gao, W. Gao, E. Cannuccia, J. Taha-Tijerina, L. Balicas, A. Mathkar, T. N. Narayanan, Z. Liu, B. K. Gupta, J. Peng, Y. Yin, A. Rubio and P. M. Ajayan, *Nano Lett.*, 2012, **12**, 3518–3525.
7 A. K. Geim and I. V. Grigorieva, *Nature*, 2013, **499**, 419.
8 J. E. Padilha, A. Fazzio and A. J. R. da Silva, *Phys. Rev. Lett.*, 2015, **114**, 066803.
9 W. Xia, L. Dai, P. Yu, X. Tong, W. Song, G. Zhang and Z. Wang, *Nanoscale*, 2017, **9**, 4324.
10 J. Oostinga, H. Heersche, X. Liu, A. F. Morpurgo and L. M. K. Vandersypen, *Nat. Mater.*, 2007, **7**, 151.
11 T. Ohta, A. Bostwick, T. Seyller, K. Horn and E. Rotenberg, *Science*, 2006, **313**, 951–954.
12 A. Ramasubramaniam, D. Naveh and E. Towe, *Phys. Rev. B: Condens. Matter Mater. Phys.*, 2011, **84**, 205325.
13 M. Kang, B. Kim, S. H. Ryu, S. W. Jung, J. Kim, L. Moreschini, C. Jozwiak, E. Rotenberg, A. Bostwick and K. S. Kim, *Nano Lett.*, 2017, **17**, 1610–1615.
14 Y. Liu, Z. Qiu, A. Carvalho, Y. Bao, H. Xu, S. J. R. Tan, W. Liu, A. H. Castro Neto, K. P. Loh and J. Lu, *Nano Lett.*, 2017, **17**, 1970–1977.
15 B. Deng, V. Tran, Y. Xie, H. Jiang, C. Li, Q. Guo, X. Wang, H. Tian, S. J. Koester, H. Wang, J. J. Cha, Q. Xia, L. Yang and F. Xia, *Nat. Commun.*, 2017, **8**, 14474.
16 T. Cheiwchanchamnangij and W. R. L. Lambrecht, *Phys. Rev. B: Condens. Matter Mater. Phys.*, 2012, **85**, 205302.
17 Z. Zhu and D. Tománek, *Phys. Rev. Lett.*, 2014, **112**, 176802.
18 J. Qiao, X. Kong, Z.-X. Hu, F. Yang and W. Ji, *Nat. Commun.*, 2014, **5**, 4475.
19 W. Li, X. Dai, J. Morrone, G. Zhang and R. Zhou, *Nanoscale*, 2017, **9**, 12025.
20 K. S. Novoselov, A. K. Geim, S. V. Morozov, D. Jiang, M. I. Katsnelson, I. V. Grigorieva, S. V. Dubonos and A. A. Firsov, *Nature*, 2005, **438**, 197.
21 K. Watanabe, T. Taniguchi, H. Kanda, D. Jiang, M. I. Katsnelson, I. V. Grigorieva, S. V. Dubonos and A. A. Firsov, *Nat. Mater.*, 2004, **3**, 404.
22 J. Mahmood, E. K. Lee, M. Jung, D. Shin, H.-J. Choi, J.-M. Seo, S.-M. Jung, D. Kim, F. Li, M. S. Lah, N. Park, H.-J. Shin, J. H. Oh and J.-B. Baek, *Proc. Natl. Acad. Sci. U. S. A.*, 2016, **113**, 7414–7419.
23 S. Yang, W. Li, C. Ye, G. Wang, H. Tian, C. Zhu, P. He, G. Ding, X. Xie, Y. Liu, Y. Lifshitz, S. Lee, Z. Kang and M. Jiang, *Adv. Mater.*, 2017, **29**, 1605625.

24 W. Kohn and L. J. Sham, *Phys. Rev.*, 1965, **140**, A1133–A1138.
25 G. Kresse and J. Furthmüller, *Comput. Mater. Sci.*, 1996, **6**, 15–50.
26 J. P. Perdew, K. Burke and M. Ernzerhof, *Phys. Rev. Lett.*, 1996, **77**, 3865–3868.
27 G. Stefan, *J. Comput. Chem.*, 2006, **27**, 1787–1799.
28 X. Chen, F. Tian, C. Persson, W. Duan and N.-x. Chen, *Sci. Rep.*, 2013, **3**, 3046.
29 H. J. Monkhorst and J. D. Pack, *Phys. Rev. B: Solid State*, 1976, **13**, 5188–5192.
30 J. Heyd, G. E. Scuseria and M. Ernzerhof, *J. Chem. Phys.*, 2003, **118**, 8207–8215.
31 A. V. Krukau, O. A. Vydrov, A. F. Izmaylov and G. E. Scuseria, *J. Chem. Phys.*, 2006, **125**, 224106.
32 P. Gava, M. Lazzeri, A. M. Saitta and F. Mauri, *Phys. Rev. B: Condens. Matter Mater. Phys.*, 2009, **79**, 165431.
33 A. A. Avetisyan, B. Partoens and F. M. Peeters, *Phys. Rev. B: Condens. Matter Mater. Phys.*, 2009, **80**, 195401.
34 W. Tang, E. Sanville and G. Henkelman, *J. Phys.: Condens. Matter*, 2009, **21**, 084204.